Available online at www.sciencedirect.com
ScienceDirect
Journal of Power Sources 161 (2006) 240–249
JOURNAL OF POWER SOURCES
www.elsevier.com/locate/jpowsour

Effect of breathing-hole size on the electrochemical species in a free-breathing cathode of a DMFC

J.J. Hwang [a,*], S.D. Wu [a], L.K. Lai [a], C.K. Chen [b], D.Y. Lai [b]

[a] *Research Center for Advanced Science and Technology, Mingdao University, Changhua 52345, Taiwan*
[b] *Department of Mechanical Engineering, National Cheng Kung University, Taiwan 701, Taiwan*

Received 15 January 2006; received in revised form 18 March 2006; accepted 28 March 2006
Available online 19 June 2006

Abstract

A three-dimensional numerical model is developed to study the electrochemical species characteristics in a free-breathing cathode of a direct methanol fuel cell (DMFC). A perforated current collector is attached to the porous cathode that breathes the fresh air through an array of orifices. The radius of the orifice is varied to examine its effect on the electrochemical performance. Gas flow in the porous cathode is governed by the Darcy equation with constant porosity and permeability. The multi-species diffusive transports in the porous cathode are described using the Stefan–Maxwell equation. Electrochemical reaction on the surfaces of the porous matrices is depicted via the Butler–Volmer equation. The charge transports in the porous matrices are dealt with by Ohm's law. The coupled equations are solved by a finite-element-based CFD technique. Detailed distributions of electrochemical species characteristics such as flow velocities, species mass fractions, species fluxes, and current densities are presented. The optimal breathing-hole radius is derived from the current drawn out of the porous cathode under a fixed overpotential.

Keywords: Direct methanol fuel cell; Free-breathing cathode; Porous; Perforated current collector

1. Introduction

Passive direct methanol fuel cells (DMFCs) have received a great deal of attention since they are considered to be a potential candidate in replacing batteries in portable electronic device applications [1–5]. In structure, they are much simpler than active ones (which have fuel pumps and oxidant supplies) and, therefore, the parasitic power penalty from the auxiliary devices is eliminated. However, the power density from passive systems is not as good as those running in an active mode due to poor transport [6–11]. It is well known that an insufficient oxygen supply to the active sites will result in uneven current distributions in the electrode which reduces the fuel cell performance. Thus, one of the challenges in the design of passive DMFCs is how to feed the electrode with reactants and remove the products from the electrode appropriately.

In this paper, the effect of the breathing-hole size on the cathode performance of a passive DMFC is studied. A staggered arrangement of circular holes is distributed on the current collector that is attached to the porous cathode. Fresh air passes into the porous cathode through these holes while the electrical current is conducted out through the solid counterpart. Conservation equations of coupled mass, momentum, species and charge are developed. The momentum conservation in the porous cathode is described by Darcy's law. The multi-species diffusion in the porous cathode is illustrated by the Stefan–Maxwell equation. The Butler–Volmer equation describes the electrochemical reaction on the surfaces of the porous cathode. A finite-element based computational fluid dynamics methodology [12,13] is employed to solve the multi-physics transports for the free-breathing cathode of a DMFC. Detailed species/electrochemical characteristics such as the flow velocity, species mass flux, species mass fraction, current density, and overpotential are presented. The electrochemical performance of various perforation sizes is derived from the amount of current that is drawn out of the porous cathode under a fixed total overpotential. The results obtained in the present study can help in understanding the local gas transport and electrochemical characteristics of a free-breathing DMFC. Also, they provide a solid basis for optimizing the geometry of the passive DMFC stack.

* Corresponding author. Tel.: +886 422540025; fax: +886 422518272.
E-mail address: azaijj@mdu.edu.tw (J.J. Hwang).

0378-7753/$ – see front matter © 2006 Elsevier B.V. All rights reserved.
doi:10.1016/j.jpowsour.2006.03.096

Nomenclature

c_i	mole concentration of the species i (mol m^{-3}), $c_i = \left[\frac{\omega_i/M_i}{\sum_j^N \omega_j/M_j}\right]\frac{P}{RT}$
D_{H_2O}	diffusivity of water vapor (m^2 s^{-1})
D_{O_2}	diffusivity of oxygen (m^2 s^{-1})
F	Faraday's constant
i_{ct}	current density (A m^{-2})
M	molecular weight (kg mol^{-1})
$\mathbf{n}$	mass flux (kg m^2 s^{-1})
p	pressure (Pa)
$p_{i,m}$	possibility of the electrolyte in the connection of the catalyst layer
$p_{i,s}$	possibility of the catalyst in the connection of the catalyst layer
r	radius of the perforation
R	universal gas constant (W mol^{-1} K^{-1})
T	temperature (K)
$\mathbf{u}$	velocity vectors (m s^{-1})
x, y, z	coordinate system, Fig. 1 (m)

Greek symbols

α	symmetric factor
ε	cathode porosity
η_t	total overpotential across the computational module (V)
κ	permeability (m^2)
μ	dynamic viscosity (m s^{-2})
ρ	density (kg m^3)
σ_l	ionic conductivity of the membrane phase (S m^{-1})
σ_s	electric conductivity of the catalyst phase (S m^{-1})
τ	tortuosity
υ_l	volume fraction of the ionic conductor (electrolyte phase) in the cathode
υ_s	volume fraction of the electronic conductor (catalyst phase) in the cathode
ϕ_l	potential of the ionic conductor (electrolyte phase) (V)
ϕ_s	potential of the electric conductor (catalyst phase) (V)
ω	mass fraction

2. The model

A typical free-breathing cathode together with a layer of electrolyte is illustrated in Fig. 1. It is common to DMFCs or microPEM fuel cells [14,15]. A staggered array of circular holes is distributed on the top surfaces of the module. They are open to the ambient. A current collector sits against the remainder of the top surfaces. A unit cell of 1.5 mm by 1.5 mm in surface area is considered (Fig. 2). The thickness of the porous cathode and the electrolyte layer is the same, i.e., 75 μm. The radius, r, of the breathing holes varies from $r = 0.4$ to 0.9 mm. The dimensions

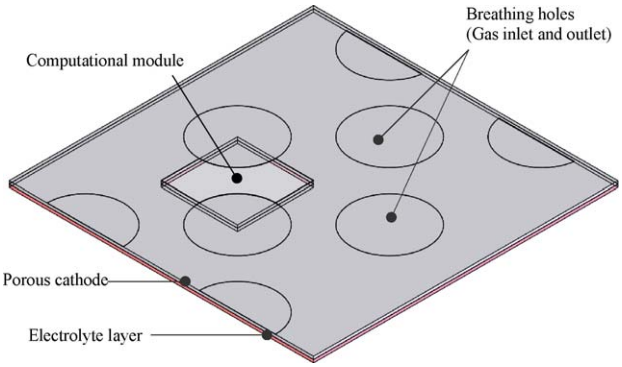

Fig. 1. Schematic drawing of passive cathode with a perforated current collector.

and coordinate system of the computational module are given in Fig. 2.

The porous cathode contains electrical conductors (catalyst), ionic conductors (the electrolyte) and the gas mixtures. The oxygen reduction reaction that takes place in the porous cathode can be expressed by the following equation:

$$O_2 + 4H^+ + 4e^- \rightarrow 2H_2O \quad (1)$$

The breathing holes are not only the entrance of fresh air but also the exit of the water vapor.

2.1. Governing equations

No reaction takes place in the electrolyte layer that connects the two electrodes of the fuel cell. The charge conservation in the electrolyte layer is given by:

$$\nabla(-\sigma_l \nabla \phi_l) = 0 \quad (2)$$

where σ_l is the ionic conductivity of the electrolyte and ϕ_l is the electrolyte potential.

In the porous cathode, the current that passes through the cathode is composed of two parts, i.e.,

$$\mathbf{i} = \mathbf{i}_s + \mathbf{i}_l \quad (3)$$

$\mathbf{i}_s$ and $\mathbf{i}_l$ are the currents flowing through the catalyst and the electrolyte, respectively. Because the porous cathode is electroneutral everywhere, no charge is built up. Thus, the charge

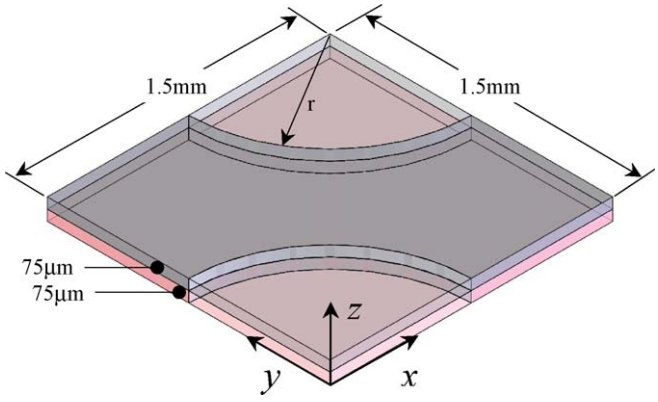

Fig. 2. Dimensions and the coordinate system of the computational module.

conservation becomes

$$\nabla \cdot \mathbf{i} = 0 \tag{4}$$

That is

$$\nabla \cdot \mathbf{i}_s = \ -\nabla \cdot \mathbf{i}_l \tag{5}$$

These two current components interact through the electrochemical reactions. What is transferred from the electrolyte to the catalyst is denoted by the (volumetric) transfer current density, i.e.,

$$\nabla \cdot \mathbf{i}_s = \ -\nabla \cdot \mathbf{i}_l = -S_a \cdot i_{ct} \tag{6}$$

where S_a is the surface area-to-volume ratio of the porous cathode and i_{ct} is the local transfer current density. Thus, by using Ohm's law, the charge conservations in the catalyst and electrolyte can be, respectively, represented by the following equations:

$$\nabla \cdot (-\sigma_{s,eff} \nabla \phi_s) = \ -S_a \cdot i_{ct} \tag{7}$$

$$\nabla \cdot (-\sigma_{l,eff} \nabla \phi_l) = S_a \cdot i_{ct} \tag{8}$$

where ϕ_s and ϕ_l are the catalyst potential and the electrolyte potentials, respectively. $\sigma_{s,eff}$ and $\sigma_{l,eff}$ are the effective electronic and ionic conductivities of the catalyst and electrolyte, respectively. They are modeled as:

$$\sigma_{s,eff} = \sigma_s(1-\varepsilon_c)\upsilon_s p_{i,s} \tag{9}$$

$$\sigma_{l,eff} = \sigma_l(1-\varepsilon_c)\upsilon_l p_{i,l} \tag{10}$$

where υ_s and υ_l are the volume fraction of the catalyst and electrolyte in the catalyst layer, respectively. $p_{i,s}$ and $p_{i,l}$ are the refer to the catalyst and electrolyte connection of the catalyst layer, respectively [16,17]. It is noted that only a long-range connection of the same particles stretch from the catalyst layer to the electrolyte which ensures good conductivity.

The species conservations for oxygen, water vapor, and nitrogen in the gas mixture are, respectively, expressed as

$$\nabla \cdot (\rho \mathbf{u} \omega_{O_2}) = \rho D_{O_2,eff} \nabla \omega_{O_2} + \frac{\rho \omega_{O_2}}{M} D_{O_2} \nabla M + S_{O_2} \tag{11}$$

$$\nabla \cdot (\rho \mathbf{u} \omega_{H_2O}) = \rho D_{H_2O,eff} \nabla \omega_{O_2} + \frac{\rho \omega_{O_2}}{M} D_{H_2O} \nabla M + S_{H_2O} \tag{12}$$

$$\omega_{N_2} = 1 - \omega_{O_2} - \omega_{H_2O} \tag{13}$$

where ρ is the density of the gas mixture, $\mathbf{u}$ the velocity vector, and M is the mole masses of the mixture. In Eqs. (11) and (12), the first term on the right-hand side represents the Fick diffusion, while the second term is the correction to enforce the Stefan–Maxwell equations on the multi-component diffusive system. The source terms of the mass balances for oxygen and water vapor are, respectively, given by:

$$S_{O_2} = -\frac{i_{ct} S_a M_{O_2}}{4F} \tag{14}$$

$$S_{H_2O} = \frac{i_{ct} S_a M_{H_2O}}{2F} \tag{15}$$

where F is the Faraday's constant. The effective diffusivities of the oxygen ($D_{O_2,eff}$) and water vapor ($D_{H_2O,eff}$) in the porous cathode follow the Bruggemann model [18,19], i.e.,

$$D_{O_2,eff} = \varepsilon^\tau D_{O_2} \tag{16}$$

$$D_{H_2O,eff} = \varepsilon^\tau D_{H_2O} \tag{17}$$

The velocity vector in Eqs. (11) and (12) is coupled to Darcy's law accordingly:

$$\mathbf{u} = -\frac{\kappa}{\mu} \nabla p \tag{18}$$

where κ is the permeability, μ the viscosity, and p is the pressure. The continuity equation for the gas flow mixture is the sum of the continuity for the three involved species, which yields:

$$\nabla \left(\rho \frac{\kappa}{\mu} \nabla p \right) = \frac{i_{ct} S_a}{4F} (M_{O_2} - 2M_{H_2O}) \tag{19}$$

The relationship between the electrochemistry and the species transport kinetics on the cathode surfaces is depicted by the Butler–Volmer equation:

$$i_{ct} = i_o \left\{ \left(\frac{c_{O_2}}{c_{O_2,ref}} \right) \exp \left[\frac{4\alpha F}{RT} (\phi_l - \phi_s) \right] - \left(\frac{c_{H_2O}}{c_{H_2O,ref}} \right)^2 \exp \left[\frac{4(1-\alpha)F}{RT} (\phi_l - \phi_s) \right] \right\} \tag{20}$$

where α is the symmetric factor, R the universal gas constant, and T is the temperature. c_{O_2} and c_{H_2O} are the concentrations of oxygen and water vapor, respectively.

2.2. Boundary conditions

The boundary conditions for the ionic current balances are insulating at all boundaries, except for the bottom of the elec-

Table 1
Electrochemical and flow characteristic data used in the present model

Expression	Symbols	Data
Exchange current density	i_o	1.0×10^{-3} A m^{-2}
Surface to volume ratio	S_a	1.0×10^{9} m^{-1}
Ambient temperature	T	353 K
Electric conductivity of the catalyst	σ_s	1000 S m^{-1}
Ionic conductivity of the electrolyte	σ_l	5.0 S m^{-1}
Dynamic viscosity of gas mixture	μ	3.0×10^{-5} m s^{-2}
Porosity of the cathode	ε	0.4
Permeability of the cathode	κ	1.0×10^{-9} m^2
Reference mole fraction of oxygen	$c_{O_2,ref}$	3.6641
Reference mole fraction of water	$c_{O_2,ref}$	3.6641
Ambient pressure	p_{in}	1.013×10^5 Pa
N_2 molecular weight	M_{N_2}	0.028 kg mol^{-1}
O_2 molecular weight	M_{O_2}	0.032 kg mol^{-1}
H_2O molecular weight	M_{H_2O}	0.018 kg mol^{-1}
Mass fraction of O_2 at inlet	$\omega_{O_2,in}$	0.233
Mass fraction of N_2 at inlet	$\omega_{N_2,in}$	0.766
Mass fraction of H_2O at inlet	$\omega_{H_2O,in}$	0.001

trolyte layer. The condition at this boundary is set to a constant ionic potential, $\phi_l = 0.5$ V. The boundaries for the electrical current balance are those that encompass the cathode sub-domain. The boundary conditions are all insulating except for the current collector boundary where the potential is set to zero, $\phi_s = 0$.

For the species balances, the boundary conditions are also those that encompass the cathode and are all insulating except for the ambient-contact boundary. The conditions at the module inlets/outlets (perforations) are given by the composition of the fresh air, $\omega_i = \omega_{i,0}$. For the momentum balance through Darcy's law, all boundaries are no slip, except for the module inlet/outlet, where the pressure is set to $p = p_{atm}$. The input data to the model is given in Table 1.

2.3. Numerical schemes

The governing equations are numerically solved by the finite element method [19,20]. Computations are performed on 8789 unstructured meshes. A grid-independence test is carried out

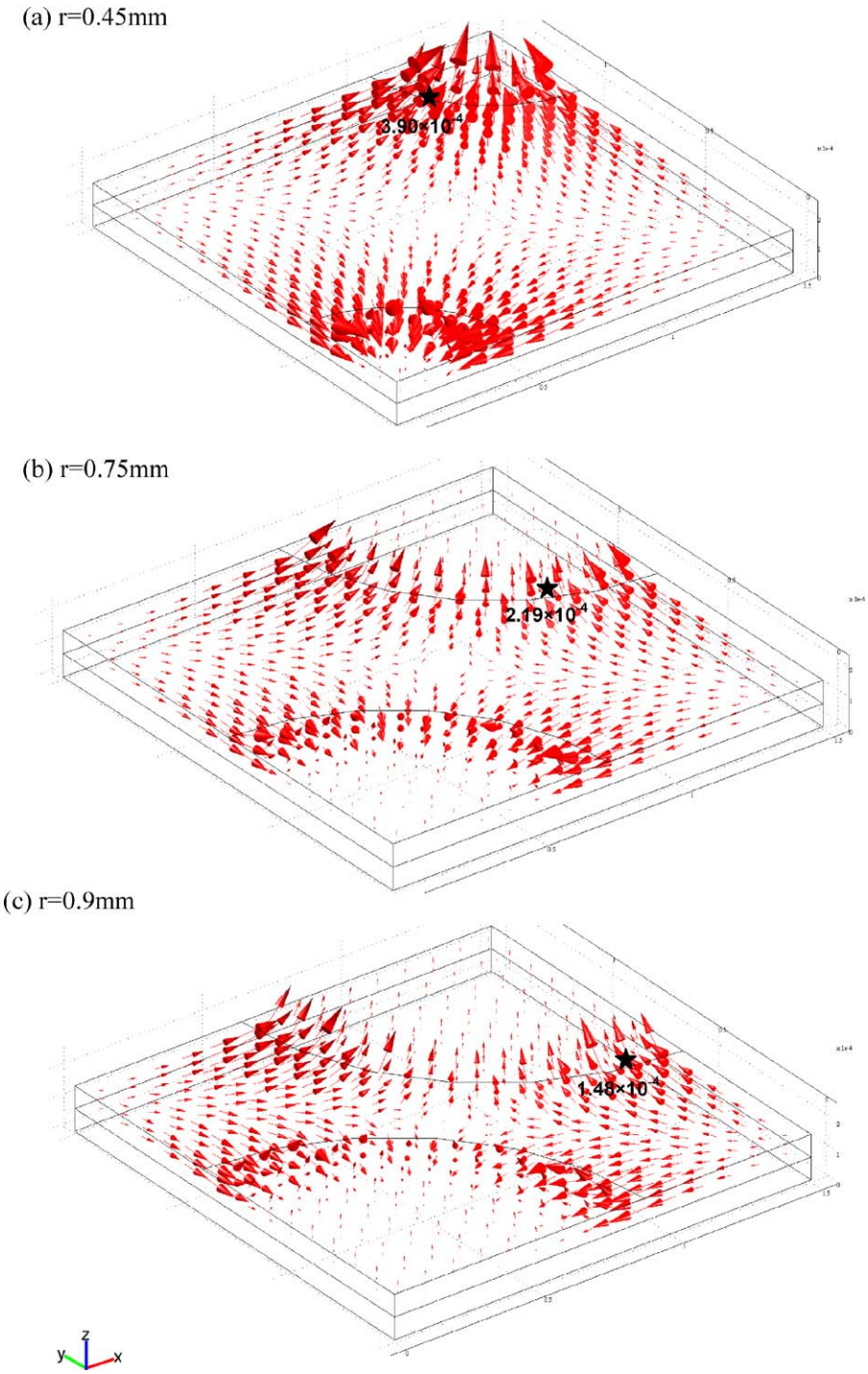

Fig. 3. Velocity distributions in porous cathode for three different perforations, the symbols on each plot represent the locations of the maximum velocity, unit: m s^{-2}.

by running three additional coarser and finer meshes. A typical simulation requires about 300 min of central processing unit time on a Pentium IV 2.8 GHz PC.

3. Results and discussion

Fig. 3 compares the gas-mixture velocity distributions in the porous cathode for three different perforation radiuses, i.e., $r = 4.5$ mm, 7.5 mm and 9.0 mm, respectively. All plots show outward flows of the gas mixture from the porous cathode to the orifices. It seems to be contrary to the paradoxical sense that the gas flow should run into the porous cathode from the ambient. Such transport phenomena are explained as follows. In the present free-breathing geometric design, the orifices act as not only the inlets for the reactants (O_2) but also the outlets for the products (H_2O). As shown in Fig. 4(a), the oxygen is delivered diffusively into the porous cathode through the orifices and then is consumed continuously by the oxygen reduction reaction (Eq. (1)). Simultaneously, water vapor is produced during the reaction and should be removed from the porous cathode. A balance of the production and consumption reveals an increase in the bulk mass of the gas mixture. Thus, the gas mixture in the porous cathode should flow outward to meet the continuity. It is further seen from Fig. 3 that significant velocity occurs around the periphery of the orifice. This is because the products (water vapor) in the reactive layer beneath the current collector accumulate and exit directly from the periphery of the orifice. In contrast, the gas-flow velocity near the orifice center is rather small because only the products beneath the orifice are removed from this region. In addition, the outlet velocity increases with decreasing orifice radius. A smaller orifice is, a higher is the outlet-flow velocity. The maximum velocities are $u_{max} = 3.895 \times 10^{-4}$ m s^{-1},

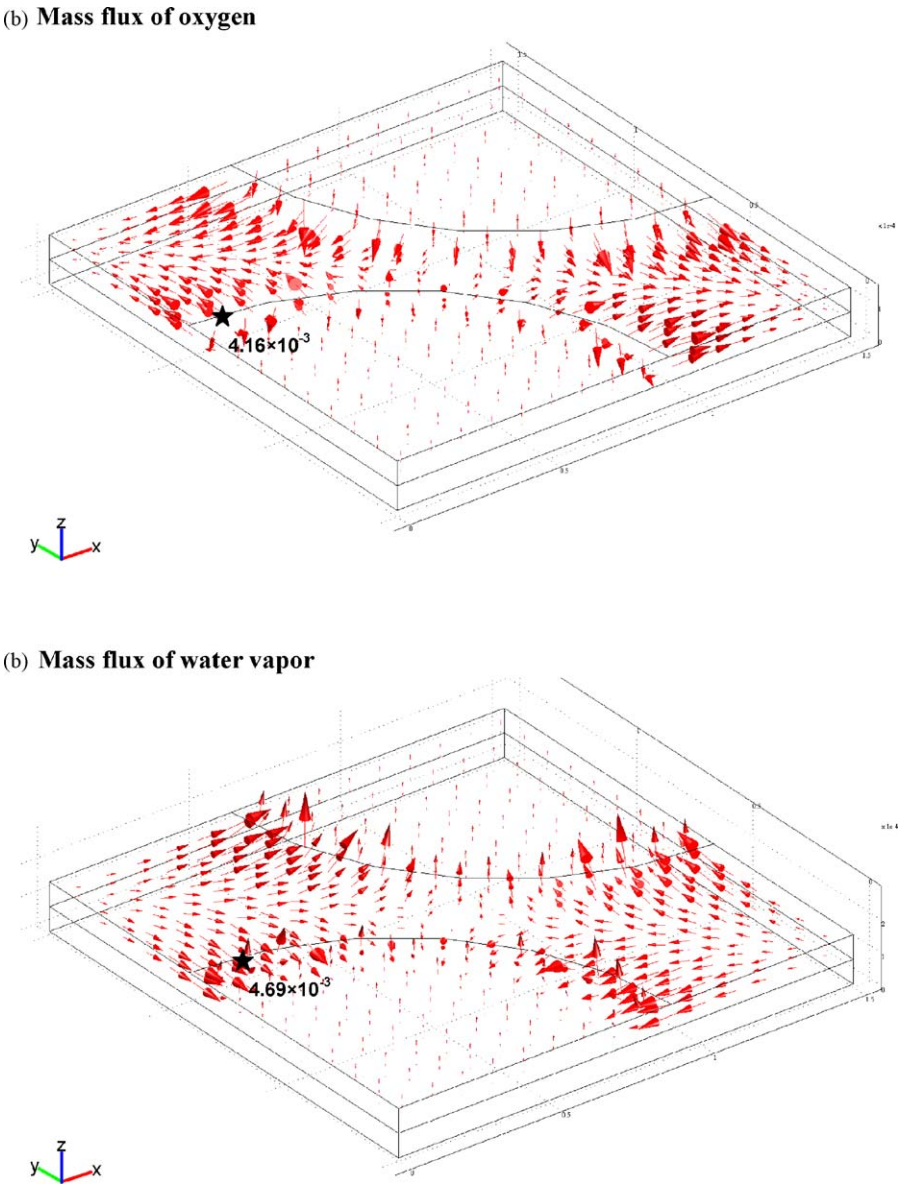

Fig. 4. Mass-flux vectors for oxygen and water vapor in the porous cathode for $r = 0.9$ mm the symbols on each plot represent the locations of the maximum flux, unit: Pa s m^{-1}.

2.187×10^{-4} m s^{-1}, and 1.482×10^{-4} m s^{-1} for the perforation radius of $r = 0.45$ mm, 0.75 mm, and 0.9 mm, respectively.

Fig. 5 shows a comparison of the iso-surfaces for the oxygen mass fraction (ω_{O_2}) in the porous cathode for three different orifice sizes. Fig. 6 shows the corresponding ω_{O_2} distributions on the bottom surface of the porous cathode ($z = 0.075$ mm), i.e., at the interface of the electrolyte layer and the porous cathode. In these two figures, the total overpotential is fixed at $\eta_t = 0.5$ V. It is seen from these plots that the projection region from the orifice has a high oxygen mass fraction. It decreases as the oxygen gradually diffuses into the cathode beneath the current collector. Two remote corners of $x = 1.5$ mm, $y = 0$ and $x = 0$, $y = 1.5$ mm have a local minimum value of ω_{O_2}, where it is too long to breath fresh air. As for the effect of the orifice size, the oxygen mass fraction increases with increasing the orifice radius in the entire porous cathode.

Fig. 7 shows the effect of the orifice radius on the overpotential distributions on the surfaces of the porous cathode. It is seen from this figure that the surface overpotential decreases with increasing the orifice radius. Near the orifices, the overpotential

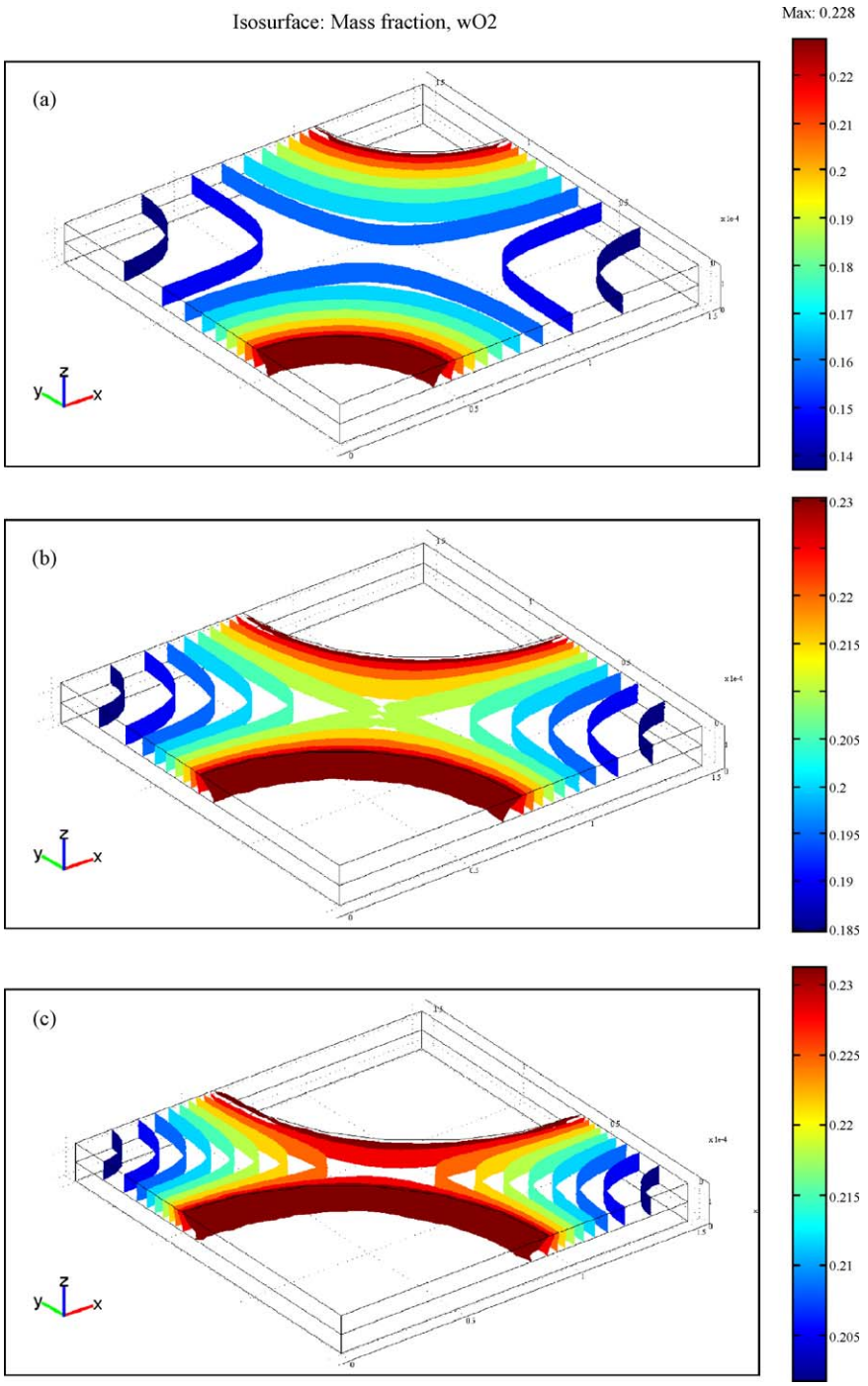

Fig. 5. Distributions of iso-mass fraction surface of oxygen for $\eta_t = 0.5$ V.

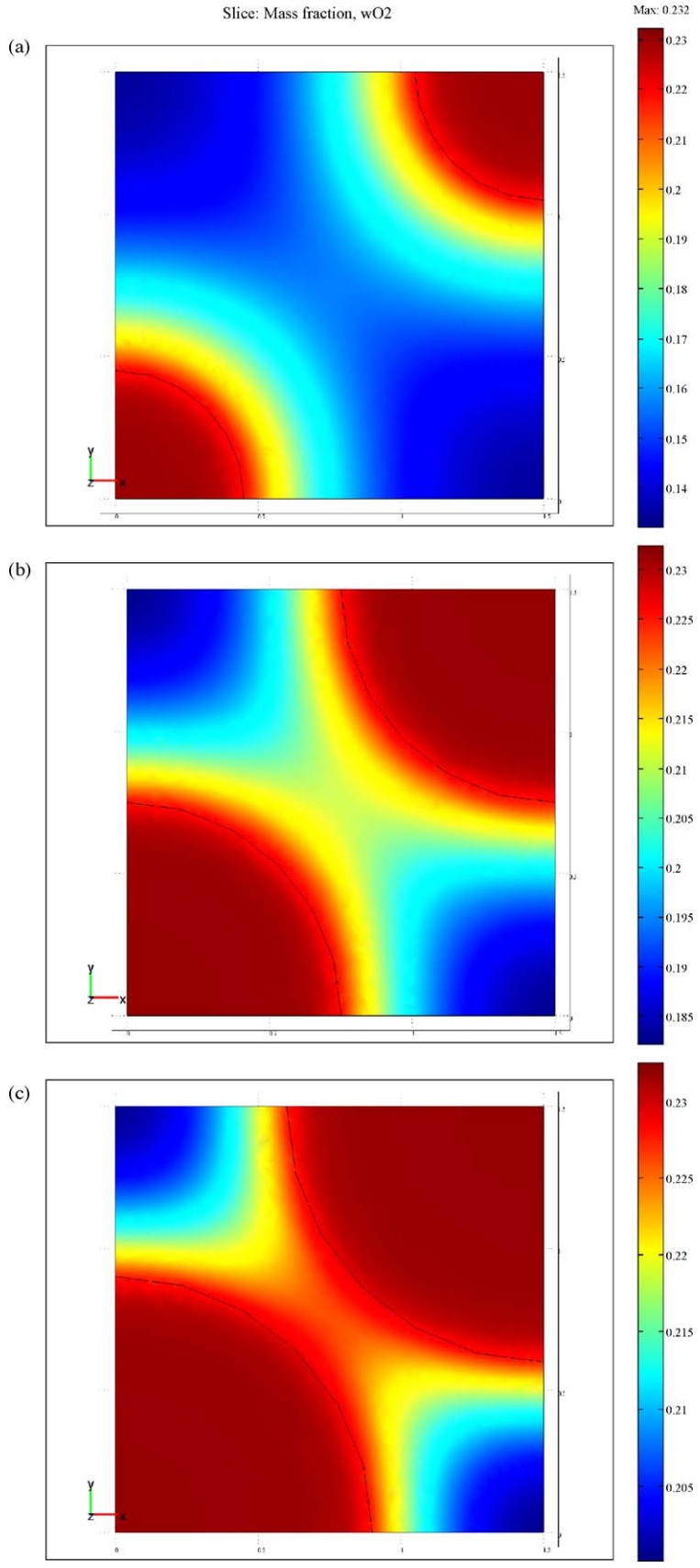

Fig. 6. Distributions of oxygen mass fractions on the plane of $z = 0.75$ mm, $\eta_t = 0.5$ V.

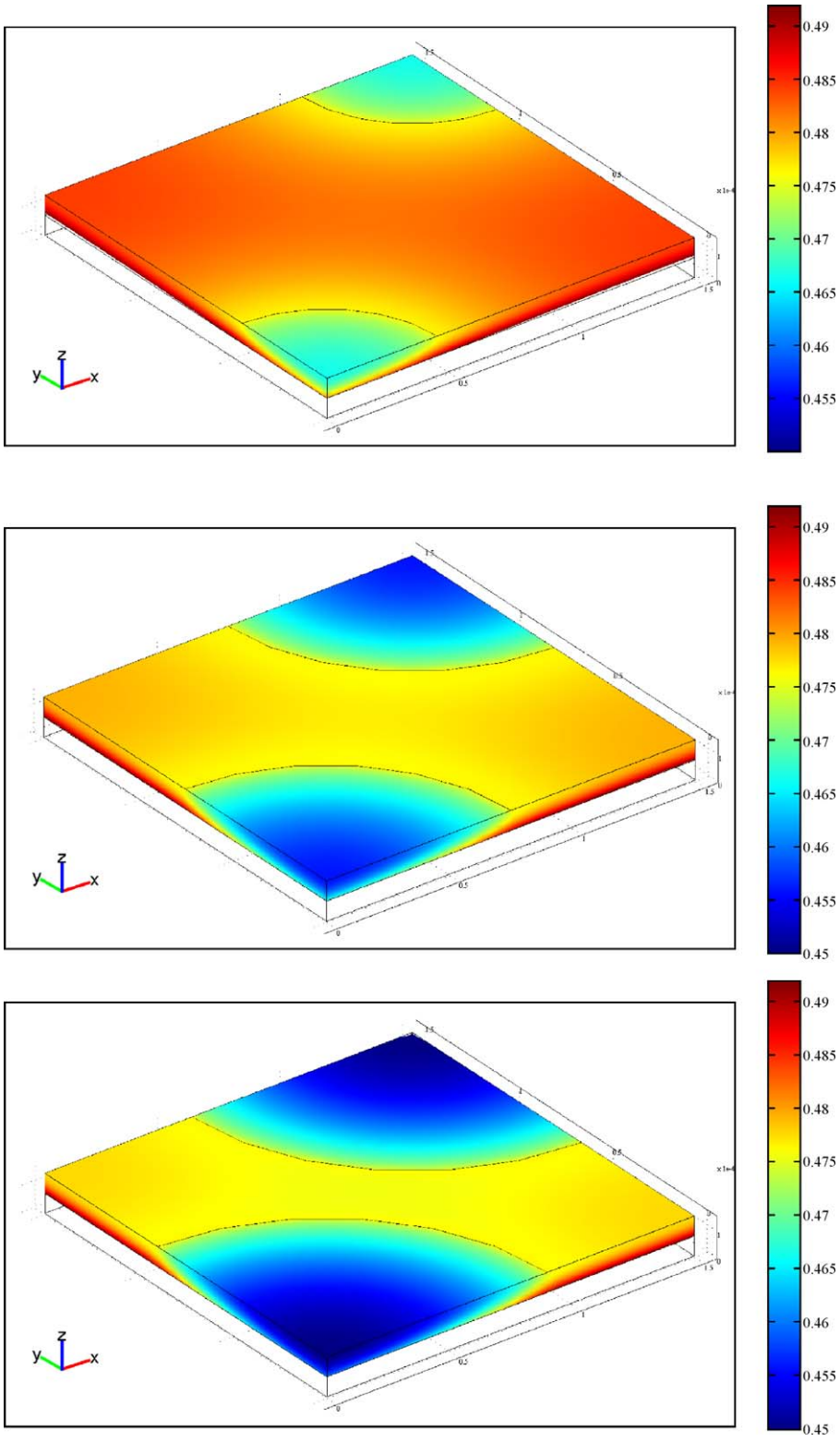

Fig. 7. Overpotential distributions on the module surfaces for three different orifice radiuses.

is small due to the lower concentration polarization. In contrast, the remote bottom corners, i.e., $x = 1.5$ mm, $y = 0$, $z = 0.75$ mm; $x = 0$, $y = 1.5$ mm, $z = 0.75$ mm, have significant overpotential. Again, this is attributed to the lowest oxygen concentration in these regions. Fig. 8 further shows the overpotential distributions along the distance between the two orifice centers. It is seen that at a fixed orifice radius, the overpotential has the lowest value at the center of the orifice. It decreases along the orifice radius and then reaches a local minimum at the middle location between the two orifices where the fresh air cannot penetrate. As for the effect of the orifice radius, it is seen from this figure that the overpotential decreases with increasing orifice radius. This

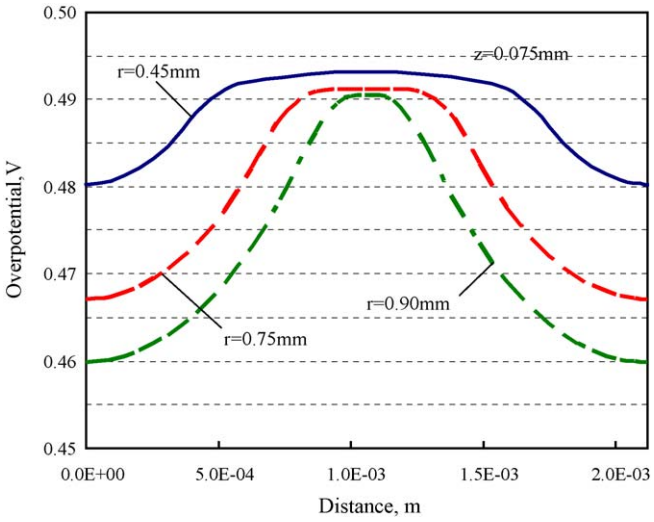

Fig. 8. Overpotential distribution along the distance between two centers of the orifices for $z = 0.075$ mm.

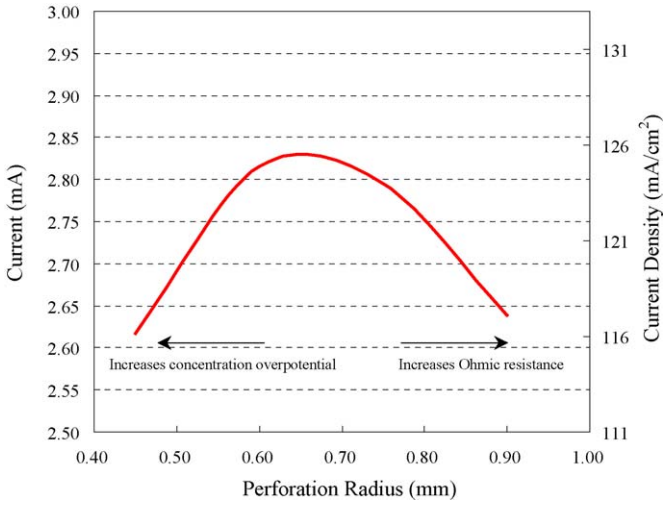

Fig. 10. Effect of orifice radius on the electrochemical performance.

is because a large breathing hole can reduce the concentration overpotential in the porous cathode.

Fig. 9 shows a comparison of the electrical current and ionic current distributions across the xz plane at $y = 0$. The arrows indicate the direction as well as the magnitude of the currents. It is seen that in the porous cathode beneath the orifice the electrical current is directed outward from the orifice center. It increases along the radial direction because of current accumulation. Near the radius edge, the electrical current turns upward to the region that subsequently is conducted by the current collector. Beneath the current collector, the electrical current goes upward and increases gradually from the bottom of the porous cathode. Again, this is because the catalyst receives transfer current from the electrolyte during the electrochemical reaction. Thus, the electrical current accumulates downstream. As for the ionic current, it is quite uniform in the electrolyte layer. In the porous cathode, by contrast, the ionic current decreases upward because the electrolyte transfers the current to the catalyst by the electrochemical reaction. As for the orifice radius which increases from $r = 0.45$ mm to $r = 0.9$ mm, two changes can be observed. First, a large breathing hole enhances the electrical current accumulation beneath the orifice. Secondly, the ionic current is enhanced by increasing the breathing hole from $r = 0.45$ mm to $r = 0.9$ mm.

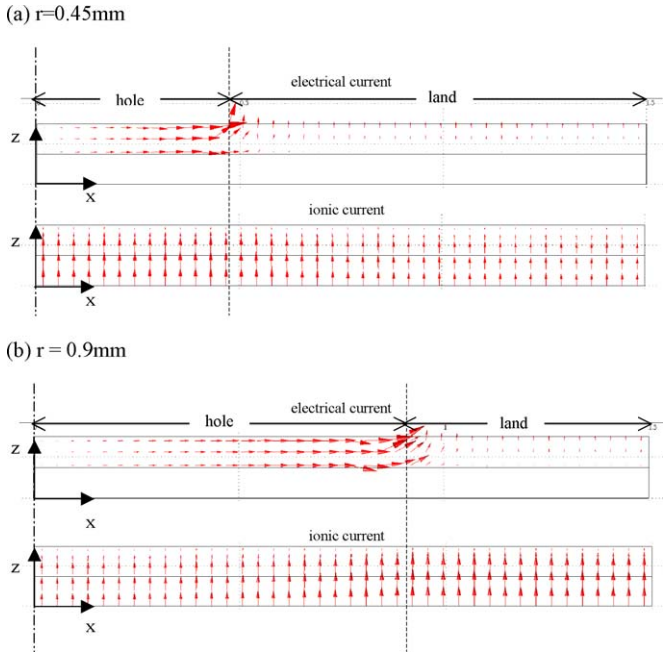

Fig. 9. Electrical current and ionic current distributions on the xz plane for $y = 0$.

Under a fixed total overpotential, the electrochemical performance can be represented by the current density that passes through the fuel cell. Fig. 10 shows the effect of orifice radius on the electrical current density passing through the computational module. The total overpotential is fixed at 0.5 V. The left ordinate is the total current drawn from the cathode, while the right ordinate is the current density. For a common basis, the current density herein is averaged over the entire area of the module (i.e., 1.5 mm by 1.5 mm) not the current-collector area only. The curve shown in Fig. 10 starts with an increase in the electrical current with increasing the breathing-hole radius from $r = 0.45$ mm. It reaches a local maximum at about $r = 0.65$ mm, and then decreases again as the breathing-hole radius further increases. As the radius of the breathing hole increases, two effects are present. First, a large opening can enhance the diffusion in the porous cathode that reduces the concentration polarization. Second, a large opening reduces the area of the current collector in contact with the porous cathode. This will result in an increase of the average current pathway from the reacting site to the current collector that increases the Ohmic drop. When the radius of the breathing hole is around $r = 0.65$ mm, these two competing effects compromise each other and show the highest current drawn out the porous cathode under a fixed total overpotential.

4. Concluding remarks

The effect of the breathing-hole size on the electrochemical performance of a free-breathing cathode of a DMFC has been

examined in detail in the present study. A three-dimensional model that couples fluid-flow fields and mass transports with the electrochemistry is developed. A finite-element based CFD method is employed to solve the coupled equations with a proper account of the electrochemical kinetics. Detailed distributions of electrochemical species characteristics such as flow velocities, species mass fraction, species flux and current density are presented. A larger breathing hole increases the Ohmic resistance penalty because the electrical current has a longer distance to the current collector from the reacting site. Simultaneously, the area in contact with the fresh air increases with increasing r that reduces the concentration polarization. The two competing effects show an optimal radius of about $r = 0.65$ mm that provides a highest current density under a fixed total overpotantial across the computational module.

Acknowledgements

This research was partly sponsored by the National Science Council of Taiwan under contract no. NSC 93-2212-E-451-002.

References

[1] A. Heinzel, C. Hebling, M. Müller, M. Zedda, C. Müller, J. Power Sources 105 (2002) 250–255.
[2] A. Bulm, T. Duvdevani, M. Philosoph, N. Rudoy, E. Pled, J. Power Sources 117 (2003) 22.
[3] D. Kim, E.A. Cho, S.A. Hong, I.H. Oh, H.Y. Ha, J. Power Sources 130 (2004) 172.
[4] B.K. Kho, I.H. Oh, S.A. Hong, H.Y. Ha, Electrochim. Acta 140 (2005) 777.
[5] J.J. Hwang, S.D. Wu, R.G. Pen, P.Y. Chen, C.H. Chao, J. Power Sources, in press.
[6] D. Chu, R. Jiang, J. Power Sources 83 (1999) 128–133.
[7] S. Morner, S.A. Klein, J. Sol. Energy Eng. 123 (2001) 225–231.
[8] M. Noponen, T. Hottinen, T. Mennola, M. Mikkola, P. Lund, J. Appl. Electrochem. 32 (2002) 1081–1089.
[9] T. Mennola, M. Mikkola, M. Noponen, T. Hottinen, P. Lund, J. Power Sources 112 (2002) 261–272.
[10] A. Schmitz, S. Wagner, R. Hahn, H. Uzun, C. Hebling, J. Power Sources 127 (2004) 197–205.
[11] T. Hottinen, M. Mikkola, P. Lund, J. Power Sources 129 (2004) 68–72.
[12] J.J. Hwang, C.K. Chen, D.Y. Lai, J. Power Sources 140 (2005) 235–242.
[13] J.J. Hwang, D.Y. Lai, C.K. Chen, J. Power Sources 143 (2005) 75–83.
[14] J.M. Moore, J.B. Lakeman, G.O. Mepsted, J. Power Sources 106 (2002) 16–20.
[15] F. Jaouena, S. Haasl, W. Wijngaart, A. Lundblada, G. Lindbergh, G. Stemme, J. Power Sources 144 (2005) 113–121.
[16] J.J. Hwang, ASME, J. Fuel Cell Sci. Technol. 2 (2005) 164–170.
[17] C.H. Kuo, P.K. Gupta, Acta Metall. Master. 39 (1995) 397.
[18] J.J. Hwang, P.Y. Chen, Int. J. Heat Mass Transfer 49 (2006) 2315.
[19] J.J. Hwang, J. Electrochem. Soc. 153 (2006) A216–A224.
[20] J.J. Hwang, D.Y. Lai, Int. J. Heat Mass Transfer 41 (1998) 979–991.